

1 Investigating the performance of simplified  
2 neutral-ion collisional heating rate in a global IT  
3 model

Jie Zhu<sup>1</sup> and Aaron J. Ridley<sup>1</sup>

---

Corresponding author: Jie Zhu, Department of Atmospheric, Oceanic and Space Sciences,  
University of Michigan, Ann Arbor, Michigan, USA. (zhjie@umich.edu)

<sup>1</sup>Department of Atmospheric, Oceanic  
and Space Sciences, University of Michigan,  
Ann Arbor, Michigan, USA.

This is the author manuscript accepted for publication and has undergone full peer review but has not been through the copyediting, typesetting, pagination and proofreading process, which may lead to differences between this version and the Version of Record. Please cite this article as doi:

10.1029/2015JA021637

December 11, 2015, 5:32pm

D R A F T

4 **Abstract.** The Joule heating rate has usually been used as an approx-  
5 imate form of the neutral-ion collisional heating rate in the thermospheric  
6 energy equation in global thermosphere-ionosphere models. This means that  
7 the energy coupling has ignored the energy gained by the ions from collisions  
8 with electrons. It was found that the globally averaged thermospheric tem-  
9 perature ( $T_n$ ) was underestimated in simulations using the Joule heating rate,  
10 by about 11% when  $F10.7=110$  sfu in a quiet geomagnetic condition. The  
11 underestimation of  $T_n$  was higher at low latitudes than high latitudes, and  
12 higher at F-region altitudes than at E-region altitudes. It was found that adding  
13 additional neutral photoelectron heating in a global IT model compensated  
14 for the underestimation of  $T_n$  using the Joule heating approximation. Adding  
15 direct photoelectron heating to the neutrals compensated for the indirect path  
16 for the energy that flows from the electrons to the ions then to the neutrals  
17 naturally, and therefore was an adequate compensation over the dayside. There  
18 was a slight dependence of the underestimation of  $T_n$  on  $F10.7$ , such that  
19 larger activity levels resulted in a need for more compensation in direct pho-  
20 toelectron heating to the neutrals to make up for the neglected indirect heat-  
21 ing through ions and electrons.

## 1. Introduction

22 The energy coupling between the ionospheric plasma and the neutral atmosphere  
23 strongly affects the global energy budget and temperature distribution of the thermo-  
24 sphere. Ionosphere-thermosphere models usually use the Joule heating approximation as  
25 the neutral-ion energy coupling term in the neutral energy equation [*Roble et al.*, 1988;  
26 *Fuller-Rowell and Rees*, 1980; *Zhu et al.*, 2005]. Various studies have shown that Joule  
27 heating [*Cole*, 1962; *Cole*, 1971] is one of the major energy sources of the upper atmo-  
28 sphere at high latitudes using satellite [*Heelis and Coley*, 1988; *Gary et al.*, 1995; *Liu and*  
29 *Lühr*, 2005] and ground-based measurements [*Banks et al.*, 1981; *Thayer*, 1998], as well  
30 as using coupled global ionosphere thermosphere models [*Barth et al.*, 2009; *Fuller-Rowell*  
31 *et al.*, 1996; *Rodger et al.*, 2001; *Deng et al.*, 2011]. *Codrescu et al.* [1995] suggested  
32 that Joule heating could be significantly underestimated by the exclusion of small-scale  
33 variability of E-field in high-latitude convection models. *Deng and Ridley* [2007] further  
34 pointed out that model resolution and the vertical differences between ion and neutral  
35 velocity were other two sources for an underestimation of Joule heating within global IT  
36 models. *Emery et al.* [1999] suggested that a corrective multiplicative factor of 2.5 of the  
37 Joule heating rate was needed for the winter hemisphere in order to account for small  
38 scale structures and rapid variability in high-latitude electric fields. Significant efforts  
39 have been made to quantify various uncertainties existing in modeling the Joule heating  
40 rate. However, despite the widespread use of the Joule heating rate as an approxima-  
41 tion of the neutral-ion collisional heating rate in the neutral energy equation, there have

42 been few studies showing how well the Joule heating rate performs in a global ionosphere  
43 thermosphere model.

44 Solar radiation in Extreme Ultraviolet (EUV) and soft X-ray wavelengths is the domi-  
45 nant energy source of the upper atmosphere. It is known that the solar radiation energy  
46 primarily goes directly into photoionization and molecular dissociation [Torr *et al.*, 1980].  
47 Photoelectrons are produced through the photoionization process, carrying photon energy  
48 in excess of the ionization threshold as kinetic energy. Photoelectrons are then responsi-  
49 ble for heating the ambient thermal electrons [Smithtro and Solomon, 2008]. Efforts have  
50 been made to develop a physical model to solve photoelectron flux and energy spectra  
51 considering transport, elastic and inelastic collisions, and energy loss to ambient electrons  
52 [Nagy and Banks, 1970; Richards and Torr, 1983; Torr *et al.*, 1990]. A parameterization  
53 of the electron volume heating rate by photoelectrons was developed by Swartz and Nisbet  
54 [1972]. An improved parameterization was further developed for application to photoelec-  
55 tron heating of ambient thermal electrons during solar flares [Smithtro and Solomon, 2008].  
56 It was suggested that neutrals were indirectly heated by photoelectrons: collisions between  
57 photoelectrons and thermal electrons produced hot electrons which heat neutrals and ions  
58 through elastic and inelastic collisions [Torr *et al.*, 1980; Roble and Emery, 1983; Aggar-  
59 wal *et al.*, 1979]. The electron-ion collisions dominate over the electron-neutral collisions  
60 above the E-region [Aggarwal *et al.*, 1979]. A constant photoelectron heating efficiency of  
61  $\sim 0.05$  has been applied in global ionosphere thermosphere models such as the Thermo-  
62 sphere Ionosphere Electrodynamics General Circulation Model (TIEGCM) [Roble *et al.*,  
63 1988; Richmond, 1995] and the Global Ionosphere Thermosphere Model (GITM) [Ridley  
64 *et al.*, 2006] in order to compensate for the discrepancy in the thermospheric temperature

65 between model results and observations [Burrell *et al.*, 2015; Maute, 2011]. However, there  
66 have been few literatures investigating whether there exists direct photoelectron heating  
67 to the neutral atmosphere, or quantifying the neutral photoelectron heating efficiency for  
68 the neutral atmosphere either by observation or by numerical calculation to the author's  
69 knowledge.

70 In this study, through the investigation of the performance of the Joule heating rate as  
71 an approximate form of the neutral-ion energy coupling rate in GITM, an explanation (or  
72 a justification) for using a photoelectron heating efficiency for the neutral atmosphere will  
73 be presented. To fully consider the neutral-ion energy coupling, a complete neutral-ion  
74 collisional heating terms need to be considered. Two forms of the neutral-ion heating  
75 rate were implemented in GITM: the simplified Joule heating rate and a more complete  
76 energy equation that allows energy flow from the electrons to the ions then to the neu-  
77 trals. The influence of the two forms of neutral-ion heating rate on the thermospheric  
78 temperature was investigated and three questions will be explored: (a) How much has  
79  $T_n$  been underestimated or overestimated by using the Joule heating as the neutral-ion  
80 energy coupling term? (b) How did the performance of the Joule heating term change  
81 with altitude, latitude, and local time? (c) How accurately has the neutral photoelectron  
82 heating used in global IT models compensated for the missing heating?

## 2. Methodology

83 The Global Ionosphere Thermosphere Model is a three-dimensional model that couples  
84 the ionosphere-thermosphere system in spherical coordinates [Ridley *et al.*, 2006]. In this  
85 study, the Weimer [2005] model was used for the high-latitude electric fields, and the  
86 Fuller-Rowell and Evans [1987] model was employed to produce the auroral precipitation

87 pattern. A dynamo electric field was solved for in a self-consistent way by using the  
 88 techniques described in *Richmond* [1995] and *Vichare et al.* [2012]. This study used the  
 89 recently updated GITM, in which the neutral, ion and electron energies are fully coupled  
 90 (J. Zhu and A. J. Ridley, Simulating electron and ion temperature in a global ionosphere  
 91 thermosphere model: validation and modeling an idealized substorm, submitted to *Journal of Atmospheric and Solar-Terrestrial Physics*, 2015).

93 The complete neutral-ion collisional heating rate can be written as [*Banks and Kockarts*,  
 94 1973; *Schunk*, 1975]:

$$Q_C = \sum_k n_k m_k \sum_t \frac{\nu_{kt}}{m_k + m_t} [3\kappa(T_i - T_n) + m_t(\mathbf{u}_n - \mathbf{u}_i)^2], \quad (1)$$

95 where  $n$ ,  $m$  and  $T$  are the number density, mass and temperature respectively,  $\mathbf{u}_n$  and  
 96  $\mathbf{u}_i$  are the neutral and ion velocities, and the subscripts  $t$  and  $k$  denote the ion and  
 97 neutral species, respectively, while the subscripts  $i$  and  $n$  denote the bulk ion and neutrals,  
 98 respectively. Specifically, the term "neutral-ion" was used for source terms in the neutral  
 99 energy equation and the term "ion-neutral" was used in the ion energy equation here.  
 100 The first term is the heat transfer rate from the ions to the neutrals, with the second  
 101 term being the neutral-ion frictional heating rate due to the velocity difference between  
 102 the two species [*Banks and Kockarts*, 1973; *Schunk*, 1975].

103 Generally, the ion temperature can be assumed to be in steady-state, and balanced by  
 104 energy coupling to both neutrals and electrons:

$$3\kappa(T_i - T_n) = m_n(\mathbf{u}_n - \mathbf{u}_i)^2 + \frac{m_i + m_n}{m_i} \frac{\nu_{ie}}{\nu_{in}} (3\kappa(T_e - T_i) + m_e(\mathbf{u}_e - \mathbf{u}_i)^2), \quad (2)$$

105 where  $\nu_{ie}$  and  $\nu_{in}$  are the collisional frequencies between ions and electrons and between  
 106 ions and neutrals, respectively. Considering  $m_e \ll m_i$ , the ion-electron frictional heating  
 107 rate can be ignored, and Equation 2 can be simplified to:

$$3\kappa(T_i - T_n) = m_n(\mathbf{u}_n - \mathbf{u}_i)^2 + \frac{m_i + m_n}{m_i} \frac{\nu_{ie}}{\nu_{in}} 3\kappa(T_e - T_i). \quad (3)$$

108 At high latitudes or on the nightside when the electron density is low,  $\nu_{ie}$  can be  
 109 much less than  $\nu_{in}$ . Thus, a balance can be approximated between the ion-neutral heat  
 110 transfer rate and the ion-neutral frictional heating rate, and the ion energy equation can  
 111 be simplified to:

$$3\kappa(T_i - T_n) \cong m_n(\mathbf{u}_n - \mathbf{u}_i)^2. \quad (4)$$

112 This assumption has been widely applied for large temporal and spatial ionospheric struc-  
 113 ture at high latitudes when the ion density is low [*St-Maurice and Hanson, 1982; Killeen*  
 114 *et al., 1984; Schunk and Nagy, 2009; Thayer and Semeter, 2004*].

This approximation can be substituted into Equation 1, so that the complete neutral-ion collisional heating rate can be written as:

$$Q_C \approx Q_J = \sum_k n_k m_k \sum_t \frac{\nu_{kt}}{m_k + m_t} [m_k(\mathbf{u}_n - \mathbf{u}_i)^2 + m_t(\mathbf{u}_n - \mathbf{u}_i)^2]. \quad (5)$$

115 This is consistent with the suggestion by *St-Maurice and Hanson [1982]* that the Joule  
 116 heating rate was twice the neutral-ion frictional heating assuming  $m_k \approx m_t$ . This equiv-  
 117 alence was confirmed by in Situ measurements by the Atmosphere Explorer satellites  
 118 around the 1980s [*St-Maurice and Hanson, 1982*].

119 Using the relation:

D R A F T

December 11, 2015, 5:32pm

D R A F T

$$n_n m_n \nu_{ni} = n_i m_i \nu_{in}, \quad (6)$$

120 the neutral-ion collisional heating rate in Equation 5 can be written as:

$$Q_J = \sum_t n_t m_t \sum_k \nu_{tk} (\mathbf{u}_n - \mathbf{u}_i)^2. \quad (7)$$

121 If the ion and electron motion perpendicular to the magnetic field is in steady state and  
 122 determined only by the Lorentz and ion drag force, the electron gyro-frequency is much  
 123 greater than the electron-neutral collisional frequency which is true above 90 km [*Brekke*,  
 124 2012; *Thayer and Semeter*, 2004; *Strangeway*, 2012],  $Q_J$  is equivalent to the Joule heating  
 125 rate:

$$Q_J = \mathbf{j} \cdot \mathbf{E}', \quad (8)$$

126 Here,  $\mathbf{j}$  is current and  $\mathbf{E}'$  is the electric field in the neutral gas frame [*Thayer and Semeter*,  
 127 2004].

128 The errors in the temporal change rate of  $T_n$  using Joule heating rate can be estimated  
 129 by subtracting the time rate of change of  $T_n$  due to  $Q_J$  from that due to  $Q_C$ . The time  
 130 rate of change of the neutral temperature due to the neutral-ion energy coupling is given  
 131 by:

$$\frac{dT_n}{dt} = \frac{Q}{\kappa \sum_k n_k m_k}, \quad (9)$$

132 where  $\kappa$  is the boltzmann constant, and  $Q$  stands for either the Complete neutral-ion  
 133 collisional heating rate as shown in Equation 1 or the Joule heating rate as shown in



134 Equation 7. For simplicity, the mean mass (i.e., number density weighted mass) was  
 135 applied for the neutrals ( $\bar{m}_n$ ) and ions ( $\bar{m}_i$ ) in the following calculation. In order to  
 136 explain the errors in the simplification in going from the more-complete equation to the  
 137 Joule heating simplification, the difference between the two can be explored and expressed  
 138 as:

$$\Delta \frac{dT_n}{dt} \propto \frac{Q_C - Q_J}{n_n \bar{m}_n \kappa}. \quad (10)$$

139  $Q_C$  in Equation 1 was simplified to:

$$Q_{C_s} = n_n \bar{m}_n \frac{\nu_{ni}}{\bar{m}_n + \bar{m}_i} [3\kappa(T_i - T_n) + \bar{m}_i(\mathbf{u}_n - \mathbf{u}_i)^2], \quad (11)$$

140 while  $Q_J$  in Equation 5 was simplified to:

$$Q_{J_s} = n_n \bar{m}_n \frac{\nu_{ni}}{\bar{m}_n + \bar{m}_i} [\bar{m}_n(\mathbf{u}_n - \mathbf{u}_i)^2 + \bar{m}_i(\mathbf{u}_n - \mathbf{u}_i)^2] \quad (12)$$

141 Substituting  $Q_{C_s}$  and  $Q_{J_s}$  into Equation 10 leads to:

$$\Delta \frac{dT_n}{dt} \propto \frac{\nu_{ni}}{\kappa(\bar{m}_n + \bar{m}_i)} [3\kappa(T_i - T_n) - \bar{m}_n(\mathbf{u}_n - \mathbf{u}_i)^2], \quad (13)$$

142 Substituting Equation 3 into Equation 13 and assuming  $\bar{m}_n \approx \bar{m}_i$  results in:

$$\Delta \frac{dT_n}{dt} \propto \frac{\nu_{ie}}{\bar{m}_i} 3(T_e - T_i). \quad (14)$$

143 Considering the electron-ion collision frequency in  $s^{-1}$  [*Schunk and Nagy, 2009*]:

$$\nu_{ei} = 5.44 \times 10^{-5} \frac{n_i Z_i^2}{T_e^{3/2}}, \quad (15)$$

144 where  $n_i$  is the ion number density in  $\text{m}^{-3}$ ,  $Z_i$  is the number of ion charge,  $T_e$  is in K and  
 145 54.4 is in  $\text{s}^{-1} \text{K}^{3/2} \text{m}^3$ , and the relation:

$$n_e m_e \nu_{ei} = n_i m_i \nu_{ie} \quad (16)$$

146 is used. Equation 14 can be further expressed as:

$$\Delta \frac{dT_n}{dt} \propto (3\kappa \frac{5.44 \times 10^{-5} Z_i^2 m_e}{\bar{m}_i^2}) \frac{n_i}{T_e^{2/3}} (T_e - T_i) \propto \frac{n_i}{T_e^{2/3}} (T_e - T_i). \quad (17)$$

147 Here, the variation of the neutral-ion collisional frequency (which is neutral-density de-  
 148 pendent) was ignored. This equation shows that the Joule heating approximation is valid  
 149 in regions in which either (a) the ion density is quite low ; or (b) the temperature dif-  
 150 ference between the ions and electrons is small. As noted by *St-Maurice and Hanson*  
 151 [1982]; *Killeen et al.* [1984]; *Schunk and Nagy* [2009]; *Thayer and Semeter* [2004], these  
 152 conditions tend to occur at high latitudes.

153 The heating rates are defined for reference below. The ion-neutral frictional heating  
 154 rate is

$$Q_F(I - N) = \sum_t n_t m_t \sum_k \frac{m_k \nu_{tk}}{m_t + m_k} (\mathbf{u}_n - \mathbf{u}_i)^2, \quad (18)$$

155 and the ion-neutral heat transfer rate is

$$Q_T(I - N) = \sum_t n_t m_t \sum_k \frac{3\kappa\nu_{tk}}{m_t + m_k} (T_i - T_n). \quad (19)$$

156 The ion-electron heat transfer rate is expressed as:

$$Q_T(I - E) = \sum_t n_t m_t \frac{3\kappa\nu_{te}}{m_t + m_e} (T_i - T_e). \quad (20)$$

157 In this study, the complete neutral-ion collisional heating rate in Equation 1 and the  
 158 Joule heating rate in Equation 7 were implemented in the Global Ionosphere Thermo-  
 159 sphere Model. First, a set of simulations were conducted during the winter solstice, i.e.,  
 160 Dec 21-23, 2012. The first simulation used a complete neutral-ion collisional heating rate  
 161 with zero photoelectron heating efficiency (PHE) (termed the Complete simulation). The  
 162 second simulation used the Joule heating rate as an approximate form of the neutral-ion  
 163 collisional heating rate with zero PHE (termed the Joule simulation). The third simula-  
 164 tion (termed the Joule simulation with 0.05 PHE), is the same as the Joule simulation  
 165 except with a PHE efficiency of 0.05. All external drivers in the three simulations were  
 166 the same and constant: the  $F10.7$  index was 110 sfu, IMF  $B_z$  was southward with the  
 167 value of  $-2$  nT and the IMF  $B_y$  was zero nT, the solar wind speed was 400 km/s, and  
 168 the hemispheric power was set to 20 GW. The dynamo solver was turned on in all the  
 169 simulations. The grid size was  $2.5^\circ$  longitude by  $1.0^\circ$  latitude. The altitudinal grid size  
 170 was stretched to about  $\frac{1}{3}$  of a scale height based on the initial thermospheric temperature  
 171 and density. Also, the same set of simulations were conducted with two different  $F10.7$ :  
 172 70 sfu and 150 sfu, in order to explore the dependence of the Joule heating approximation

173 on solar irradiance and justify the photoelectron heating efficiency used to compensate  
174 the missing heating.

### 3. Results

#### 3.1. Comparison between the Complete and Joule simulations

175 Figure 1 shows the temporal variation of the globally volume-averaged neutral temper-  
176 ature over three simulation days for the three cases. The globally averaged temperature  
177 was plotted to illustrate the evolution of the simulations into a steady state. In all three  
178 cases, the globally averaged  $T_n$  decreased quickly during the first 5 hours, increased grad-  
179 ually and leveled off at the beginning of the third day.  $T_n$  dropped in the beginning of the  
180 simulation because GITM does not assume a hydrostatic solution [Ridley *et al.*, 2006],  
181 and it is initialized with MSIS [Hedin *et al.*, 1977], which does not have a perfectly hy-  
182 drostatic balance. There were massive modifications of the dynamics that took place over  
183 the beginning of the simulations.  $T_n$  in the Joule simulation leveled off at around 740 K,  
184 which was about 90 K ( $\sim 11\%$ ) lower than the Complete simulation. This was expected  
185 because the Joule heating rate did not account for the ion-electron heat transfer in the ion  
186 thermal equation. This resulted in an underestimation of  $T_i - T_n$  as shown in Equation 4,  
187 thus leading to a lower neutral-ion heat transfer rate for the neutrals. This phenomenon  
188 tends to occur in the dayside F-region where the ion densities are large and the electron  
189 temperature becomes progressively larger than the ion temperature [Roble, 1975]. The  
190 third simulation, which is the normal method in global IT models, used the Joule heating  
191 rate with a non-zero neutral photoelectron heating efficiency. Different PHE values were  
192 tested (not shown here) and it was found that a Joule simulation with PHE equal to 0.05

193 had approximately the same globally averaged  $T_n$  as the Complete simulation, as shown  
194 by the dashed line in Figure 1.

195 Figure 2 shows the comparison of the  $T_n$  distribution between the three simulations.  
196 The top panels show the global horizontal distribution at 300 km of  $T_n$  for the three  
197 cases. The Joule simulation (i.e., the middle panel) shows a similar distribution of the  
198 neutral temperature as the Complete simulation (i.e., the leftmost panel), however, a  
199 difference of about 100 K existed globally at 300 km between the Complete and Joule  
200 simulations. Although it was expected that it would be the dayside where the Joule  
201 heating rate most deviated from the complete neutral-ion collisional heating rate, there  
202 was also about 100 K difference in the nightside F-region. This was due to neutral winds  
203 advecting the increased temperature from the dayside to the nightside. The comparison  
204 of  $T_n$  at 180° longitude (middle) and at 300-km altitude above 50 ° latitude (bottom)  
205 were shown in Figure 2. Large temperature differences are observed in these cuts as well.  
206 By increasing the photoelectron heating efficiency to 0.05, the Joule simulation with 0.05  
207 PHE, as shown in the third column, showed a similar global distribution as the Complete  
208 simulation excluding photoelectron heating for the neutrals.

209 The compensation for the underestimation of  $T_n$  in the Joule simulation by the neutral  
210 photoelectron heating efficiency was not a coincidence. The approximation of the neutral-  
211 ion energy coupling by the Joule heating rate is based on the assumption that the ion  
212 temperature is balanced between the energy exchange term and the frictional heating  
213 term with the neutrals. However, the heating by ambient electrons could be a non-trivial  
214 heat source where the electron density is high, i.e., on the dayside and the F-region at  
215 high latitudes [*St-Maurice and Hanson, 1982; Killeen et al., 1984*]. In these regions,  $T_i$

could deviate from the energy balance assumption as shown in Equation 4 due to the ion-electron energy coupling. In other words,  $T_i$  was underestimated in the Joule heating rate as a form of the neutral-ion energy coupling. Therefore, the Joule heating rate turned out to be smaller than the complete neutral-ion collisional heating rate in these regions. Furthermore, the difference between the Joule heating rate and the complete neutral-ion collisional heating rate, most likely originates from photoelectrons. This is because photoelectron heating is one of the major heat sources for the ambient thermal electrons on the dayside [Nagy and Banks, 1970; Rasussen et al., 1988; Smithtro and Solomon, 2008]. The thermal electrons heated through collisions with photoelectrons subsequently transfer thermal energy to ions, leading to a deviation from the neutral energy balance assumption of  $T_i$ . Therefore, the non-zero photoelectron heating efficiency used to calculate  $T_n$  applied in the case using the Joule heating rate (i.e., the simplified neutral-ion collisional heating rate), mimicked the indirect heating process from photoelectrons to neutrals (through the ions) as a direct heating process.

Figure 3 shows the percentage difference of the neutral temperature between the Complete simulation and the Joule simulation, as expressed in Equation 10, at 00 UT on Dec 24 (i.e., the end of the last simulation day) at 140 km, 250 km and 400 km. At 140 km, the difference was within 8%, and the northern polar region had a higher percentage difference than other regions. At 250 km, the difference increased to approximate 12% in the northern hemisphere, and about 8% in the southern hemisphere. At 400 km, the percentage difference maximized at around 15% in the low-latitude region, which was consistent with *St-Maurice and Hanson* [1982]; *Killeen et al.* [1984]; *Schunk and Nagy* [2009], who found that the ion-electron energy coupling played a less important role for the ion temperature

239 at high latitudes than it did at low and middle latitudes because the electron density was  
240 generally lower at high latitudes. Specifically,  $T_n$  was underestimated by about 10-12%  
241 in the polar regions, and by about 6% on the nightside in the Joule simulation. It was  
242 also found that the percentage difference in  $T_n$  was higher around the F-region (400 km)  
243 than around the E-region (140 km). This could be caused by two reasons: (a) the E-  
244 region electron density was generally lower than the F-region density, thus the E-region  
245 ion temperature can be better approximated by a balance through energy coupling with  
246 the neutrals than the F-region ion temperature; (b) the neutral atmosphere decreases  
247 with altitude, which makes the thermosphere at E-region altitudes more difficult to heat  
248 through neutral-ion collisional heating (or Joule heating) [Deng *et al.*, 2011].

249 In Figure 4, the colored contours show the difference of the time rate of change of the  
250 neutral temperature due to the neutral-ion energy coupling between the Complete and  
251 the Joule simulations at 140 km, 250 km and 400 km. The difference was about two  
252 orders smaller at 140 km than at 250 km or 400 km, and it was negative around the  
253 polar auroral bands at 140km where the ion temperature was slightly higher than the  
254 electron temperature due to the large frictional heating with the neutrals. As shown in  
255 Equation 17, when  $T_i$  becomes higher than  $T_e$ , the difference of the heating rate becomes  
256 negative, meaning that the Joule heating approximation would cause excess heating in  
257 these locations. The vertical profile of the ion-neutral frictional heating will be further  
258 discussed below. The model limits the electron temperature so that it can be not less than  
259 90% of the ion temperature for stability purposes. At 250 km, the difference reached a peak  
260 around 20°- 45° latitude on the dayside, and decreased towards both polar regions. At  
261 400 km, the difference maximized around the geographic equator and generally decreased

with latitude, but was relatively large on the dayside and weak on the nightside. There was also a localized maximum in the auroral zone in the southern hemisphere, which could be due to a large deviation of  $T_i$  from the energy balance assumption in the auroral band with high electron densities.

Equation 17 shows that the difference between the complete neutral-ion collisional heating and the Joule heating rate is proportional to  $\frac{n_i}{T_e^{3/2}}(T_e - T_i)$ . This term is contoured by the dotted lines in Figure 4. The contour of this proportional term generally agrees with that of difference in the time rate of change of  $T_n$  at 250 km and 400 km, which, once again, indicates that the difference between the complete neutral-ion collisional heating rate and the Joule heating rate resulted from the lack of consideration of the ion-electron energy coupling in the Joule heating rate.

One feature to note about the global distribution of  $T_n$  is that the percentage difference of  $T_n$  in Figure 3 was greater in the northern hemisphere than in the southern hemisphere. This was caused by two factors. First, as shown in Figure 2, the southern hemisphere was generally warmer than the northern hemisphere in December. A greater temperature denominator led to a smaller percentage difference even assuming a similar  $T_n$  difference between the two hemispheres. Second, the difference of the time rate of change in the neutral temperature, as shown in Figure 4, was generally greater in the northern hemisphere than in the southern hemisphere at 250 km, which indicates a greater  $T_n$  difference in the northern hemisphere.

There were some slight inconsistencies between the colored contour and the line contour at 400 km, which is expected because assumptions have been made in the derivation for Equation 17, such as using mean masses for simplification, equality of the mean masses



285 between the ions and neutrals and assuming constant ion mean mass. Further, neutral  
286 density variations were assumed to be negligible. The uncertainty of these assumptions  
287 could increase in the F-region where transport processes become important, and the vari-  
288 ations in mass density could become larger.

289 Figure 5 shows altitudinal profiles of the three major ion thermal sources and losses:  
290 the ion-electron heat transfer  $Q_T(I - E)$ , the ion-neutral frictional heating rate  $Q_F(I - N)$   
291 and the negative ion-neutral heat transfer term  $-Q_T(I - N)$  as presented in Equations 18-  
292 20 at three different locations. On the dayside, the ion temperature was approximately  
293 balanced by the ion-neutral energy coupling below 150 km altitude (i.e., energy gained by  
294 frictional heating was lost by heat transfer). The ion-electron heat transfer rate increased  
295 quickly with altitude and the ion temperature became a balance between the ion-electron  
296 and ion-neutral heat transfer rates around the F-region. The transition region of the  
297 energy balance is at approximate 180 km. This means that the Joule heating rate is  
298 a good approximation of the neutral-ion collisional heating rate in the E-region on the  
299 dayside, but not in the F-region. In the polar region, the ion energy balance was primarily  
300 between the frictional heating and heat transfer to the neutrals, until the electron heat  
301 transfer became a dominant source of energy above around 350 km. This shows that the  
302 Joule heating rate is a relatively good approximation in the high-latitude region below 350  
303 km. On the nightside, the ion-electron heat transfer was one to two orders of magnitude  
304 smaller than the other two terms throughout most of the plotted altitudes. Thus, the  
305 Joule heating rate was always a good approximate form of the neutral-ion collisional  
306 heating rate on the nightside. The frictional heating rate (i.e., yellow line) had a peak  
307 in the E-region. This indicates a large heat source for ions by friction with neutrals in

308 this region, such that  $T_i$  could be greater than  $T_e$ . This helps to explain the negative  
309 ion-electron heating rate around 100 km in the polar region and on the nightside. Note  
310 that on the nightside between the E-region and F-region, the ion temperature equation is  
311 balanced by other terms, such as thermal conduction, instead of only being balanced by  
312 friction and heat transfer.

### 3.2. $F10.7$ Dependence

313 Considering the underestimation of  $T_n$  by the Joule heating rate was mainly caused by  
314 the neglect of the indirect heating from electrons to neutrals (through ions) and photo-  
315 electron heating was the main way to make up this short fall, it may be expected that the  
316 performance of the Joule heating rate (with the 5% PHE) was solar-condition dependent.  
317 Figure 6 shows the evolution of  $T_n$  of the same set of simulations as in Figure 1 but with  
318  $F10.7 = 70$  sfu (left panel) and  $F10.7 = 150$  sfu (right panel). When the solar activity  
319 was low (i.e.,  $F10.7 = 70$  sfu), the global averaged  $T_n$  was underestimated by about 50  
320 K ( $\sim 7\%$ ) compared with the Complete simulation in steady state (i.e., at the end of the  
321 three simulation days). A photoelectron heating efficiency of 0.035 for the neutral at-  
322 mosphere compensated for the indirect heating. When the solar radiance was high (i.e.,  
323  $F10.7 = 150$  sfu), the Joule simulation underestimated the global averaged  $T_n$  by about  
324 140 K ( $\sim 14\%$ ), which could be compensated by a neutral photoelectron heating efficiency  
325 of 0.07. During a medium solar condition with  $F10.7 = 110$  sfu, as shown in Figure 1,  
326 the global averaged  $T_n$  in the Joule simulation was approximately 90 K ( $\sim 11\%$ ) cooler  
327 than it was in the Complete simulation, which required a photoelectron heating efficiency  
328 of 0.05 for compensation. These simulation results suggest a linear relation possibly ex-  
329 isting between  $F10.7$  and the performance of the Joule heating rate. An increase of 10

330 sfu of  $F10.7$  caused about 1% underestimation of  $T_n$  in a simulation using Joule heating  
331 rate with no photoelectron heating. The photoelectron heating efficiency increased by  
332 0.015 when  $F10.7$  increased from 70 sfu to 110 sfu, and increased by 0.02 when  $F10.7$   
333 was increased by 40 from 110 sfu to 150 sfu. This indicates that the PHE for the neutral  
334 atmosphere that was required for compensating  $T_n$  in Joule simulations tended to increase  
335 faster with  $F10.7$  during high solar conditions, and the electron-ion heat transfer becomes  
336 more important nonlinearly as solar activity increases.

#### 4. Discussion and Conclusion

337 This paper has discussed the performance of the Joule heating rate as an approximate  
338 form of the neutral-ion collisional heating rate in the neutral energy equation in the  
339 Global Ionosphere Thermosphere Model. This approximation was valid where the ion-  
340 electron collisional heating was negligible and the ion temperature could be approximated  
341 by a balance between energy coupling with the neutrals. It has been shown that the  
342 global average thermospheric temperature was underestimated by  $\sim 11\%$  in the Joule  
343 simulation at solar medium (i.e.,  $F10.7$  equal to 110 sfu) and quiet geomagnetic conditions.  
344 The percentage difference of  $T_n$  between the two simulations generally decreased from  
345 the dayside to the nightside, and from high to low altitudes. At 400 km, the Joule  
346 approximation underestimated the neutral temperature by about 15% on the dayside, by  
347 about 10-12% in the polar regions, and by about 6% on the nightside. The discrepancy  
348 between the Joule heating rate and the Complete neutral-ion collisional heating rate is  
349 mainly due to the neglect of the ion-electron heating in the ion energy equation. However,  
350 the ion-electron energy coupling can be a non-trivial thermal source for ions in the dayside  
351 F-region and in the higher-altitude polar region.

352 By increasing the photoelectron heating efficiency of the neutral atmosphere, the under-  
353 estimation of  $T_n$  was compensated for quite adequately. A global ionosphere-thermosphere  
354 model that used the Joule heating rate as an approximation of the neutral-ion energy  
355 coupling, usually applied a PHE for the neutral atmosphere to match model results with  
356 observations. However, there has been few studies quantifying the direct heating from  
357 photoelectrons to the neutrals. It was found that there existed a roughly linear relation  
358 between the performance of the Joule heating approximation and solar activity. Higher  
359  $F10.7$  led to a larger discrepancy in  $T_n$  in a simulation using Joule heating rate without the  
360 employment of a neutral photoelectron heating efficiency. The compensating neutral PHE  
361 increased with solar activity as well. It appeared that the indirect heating of neutrals by  
362 electrons increased more efficiently at a high level of solar activity. Beside solar activity,  
363 solar wind condition and particle precipitation at high latitude could possibly affect the  
364 performance of the Joule heating rate because the convection pattern and auroral activity  
365 could effectively change the dynamics of the ionosphere and thermosphere. Further study  
366 is needed to investigate the performance of the Joule heating approximation during geo-  
367 magnetic disturbances. A global IT model should be careful when using the Joule heating  
368 rate as an approximate form of the neutral-ion collisional heating rate. Using a fixed  
369 neutral PHE to compensate for the loss of the indirect heating from thermal electrons to  
370 neutrals may not be proper because the indirect heating from electrons to neutrals can be  
371  $F10.7$  dependent. It should also be noted that compensating for one heating source with  
372 another may allow quantities such as orbit-averaged mass density to compare quite well  
373 with measurement. In addition, since the main area of the temperature difference was on  
374 the dayside, and the photoelectron heating also worked on the dayside, any data-model

375 differences caused by issues using the photoelectron heating instead of the complete equa-  
376 tion set would be quite subtle during quiet times, as evidence by the comparisons shown  
377 here between the two simulations.

378 **Acknowledgments.** This work was partially supported by NASA Grant NNX09AJ59G,  
379 and NSF grants AGS1242787 and AGS1138938. We would like to acknowledge high-  
380 performance computing support from Yellowstone (ark:/90890) provided by NCAR's  
381 Computational and Information Systems Laboratory, sponsored by the National Sci-  
382 ence Foundation. We would also like to thank NASA's supercomputers, Pleiades  
383 (<http://www.nas.nasa.gov/hecc/resources/pleiades.html>) for conducting the sim-  
384 ulations in this study. The GITM simulation data for this case are available upon request  
385 from the authors.

## References

- 386 Aggarwal, K., N. Nath, and C. Setty (1979), Collision frequency and transport properties  
387 of electrons in the ionosphere, *Planetary and Space Science*, 27(6), 753–768.
- 388 Banks, P., J. Foster, and J. Doupanik (1981), Chatanika radar observations relating to the  
389 latitudinal and local time variations of Joule heating, *Journal of Geophysical Research:*  
390 *Space Physics (1978–2012)*, 86(A8), 6869–6878.
- 391 Banks, P. M., and G. Kockarts (1973), *Aeronomy*, Academic Press.
- 392 Barth, C., G. Lu, and R. Roble (2009), Joule heating and nitric oxide in the thermosphere,  
393 *Journal of Geophysical Research: Space Physics (1978–2012)*, 114(A5).
- 394 Brekke, A. (2012), *Physics of the upper polar atmosphere*, Springer Science & Business  
395 Media.

- 396 Burrell, A. G., A. Goel, A. J. Ridley, and D. S. Bernstein (2015), Correction of the photo-  
397 electron heating efficiency with the global ionosphere-thermosphere model using retro-  
398 spective cost model refinement, *Journal of Atmospheric and Solar-Terrestrial Physics.*,  
399 *124*, 30–38, doi:10.1016/j.jastp.2015.01.004.
- 400 Codrescu, M., T. Fuller-Rowell, and J. Foster (1995), On the importance of E-field vari-  
401 ability for Joule heating in the high-latitude thermosphere, *Geophysical Research Let-*  
402 *ters*, *22*(17), 2393–2396.
- 403 Cole, K. (1971), Electrodynamical heating and movement of the thermosphere, *Planetary*  
404 *and Space Science*, *19*(1), 59–75.
- 405 Cole, K. D. (1962), Joule heating of the Upper Atmosphere, *Australian Journal of Physics*,  
406 *15*, 223, doi:10.1071/PH620223.
- 407 Deng, Y., and A. J. Ridley (2007), Possible reasons for underestimating Joule heating in  
408 global models: E field variability, spatial resolution, and vertical velocity, *Journal of*  
409 *Geophysical Research: Space Physics (1978–2012)*, *112*(A9).
- 410 Deng, Y., T. J. Fuller-Rowell, R. A. Akmaev, and A. J. Ridley (2011), Impact of the altitu-  
411 dinal Joule heating distribution on the thermosphere, *Journal of Geophysical Research:*  
412 *Space Physics (1978–2012)*, *116*(A5).
- 413 Emery, B. A., C. Lathuillere, P. G. Richards, R. G. Roble, M. J. Buonsanto, D. J. Knipp,  
414 P. Wilkinson, D. P. Sipler, and R. Niciejewski (1999), Time dependent thermospheric  
415 neutral response to the 2-11 november 1993 storm period, *Journal of Atmospheric and*  
416 *Solar-Terrestrial Physics.*, *61*, 329–350, doi:10.1016/S1364-6826(98)00137-0.
- 417 Fuller-Rowell, T., M. Codrescu, H. Rishbeth, R. Moffett, and S. Quegan (1996), On the  
418 seasonal response of the thermosphere and ionosphere to geomagnetic storms, *Journal*

- 419 of *Geophysical Research: Space Physics (1978–2012)*, 101(A2), 2343–2353.
- 420 Fuller-Rowell, T. J., and D. S. Evans (1987), Height-integrated pedersen and hall con-  
421 ductivity patterns inferred from the tiros-noaa satellite data, *Journal of Geophysical*  
422 *Research*, 92, doi:10.1029/JA092iA07p07606.
- 423 Fuller-Rowell, T. J., and D. Rees (1980), A three-dimensional time-dependent global  
424 model of the thermosphere, *Journal of the Atmospheric Sciences*, 37, 2545, doi:10/  
425 1980;37:2545-2567.
- 426 Gary, J., R. Heelis, and J. Thayer (1995), Summary of field-aligned Poynting flux obser-  
427 vations from de 2, *Geophysical research letters*, 22(14), 1861–1864.
- 428 Hedin, A. E., et al. (1977), A global thermospheric model based on mass spectrometer  
429 and incoherent scatter data msis, 1. n2 density and temperature, *Journal of Geophysical*  
430 *Research*, 82(16), 2139–2147, doi:10.1029/JA082i016p02139.
- 431 Heelis, R., and W. Coley (1988), Global and local Joule heating effects seen by de 2,  
432 *Journal of Geophysical Research: Space Physics (1978–2012)*, 93(A7), 7551–7557.
- 433 Killeen, T. L., P. B. Hays, G. R. Carignan, R. H. Heelis, W. B. Hanson, N. W. Spencer,  
434 and L. H. Brace (1984), Ion-neutral coupling in the high-latitude f region: Evaluation  
435 of ion heating terms from dynamics explorer 2, *Journal of Geophysical Research*, 89,  
436 7495, doi:10.1029/JA089iA09p07495.
- 437 Liu, H., and H. Lühr (2005), Strong disturbance of the upper thermospheric density due to  
438 magnetic storms: Champ observations, *Journal of Geophysical Research: Space Physics*  
439 *(1978–2012)*, 110(A9).
- 440 Maute, A. (2011), *TIEGCM V 1.94 Model Description*, National Center for Atmospheric  
441 Research, Boulder, CO.

- 442 Nagy, A., and P. Banks (1970), Photoelectron fluxes in the ionosphere, *Journal of Geo-*  
443 *physical Research*, 75(31), 6260–6270.
- 444 Rasussen, C. E., J. J. Sojka, R. W. Schunk, V. B. Wickwar, and O. de la Beaujardiere  
445 (1988), Comparison of simultaneous chatanika and millstone hill temperature measure-  
446 ments with ionospheric model predictions, *Journal of Geophysical Research*, 93, 1922,  
447 doi:10.1029/JA093iA03p01922.
- 448 Richards, P., and D. Torr (1983), A simple theoretical model for calculating and param-  
449 eterizing the ionospheric photoelectron flux, *Journal of Geophysical Research: Space*  
450 *Physics (1978–2012)*, 88(A3), 2155–2162.
- 451 Richmond, A. D. (1995), Ionospheric electrodynamics using magnetic apex coordinates,  
452 *Journal of Geomagnetism and Geoelectricity*, 47.
- 453 Ridley, A., Y. Deng, and G. Tòth (2006), The global ionosphere-thermosphere model,  
454 *Journal of Atmospheric and Solar-Terrestrial Physics.*, 68, 839, doi:10.1016/j.jastp.  
455 2006.01.008.
- 456 Roble, R. (1975), The calculated and observed diurnal variation of the ionosphere  
457 over millstone hill on march 23-24, 1970, *Planet. Space Sci.*, 23, 1017, doi:10.1016/  
458 0032-0633(75)90192-0.
- 459 Roble, R., and B. Emery (1983), On the global mean temperature of the thermosphere,  
460 *Planetary and Space Science*, 31(6), 597–614.
- 461 Roble, R. G., E. Ridley, A. Richmond, and R. Dickinson (1988), A coupled thermo-  
462 sphere/ionosphere general circulation model, *Geophysical Research Letters*, 15, 1325,  
463 doi:10.1029/GL015i012p01325.



- 464 Rodger, A., G. Wells, R. Moffett, and G. Bailey (2001), The variability of Joule heating,  
465 and its effects on the ionosphere and thermosphere, in *Annales Geophysicae*, vol. 19,  
466 pp. 773–781.
- 467 Schunk, R., and A. Nagy (2009), *Ionospheres: Physics, Plasma Physics, and Chemistry*,  
468 Cambridge University Press.
- 469 Schunk, R. W. (1975), Transport equations for aeronomy, *Planetary and Space Science*,  
470 *23*, 437–485, doi:10.1016/0032-0633(75)90118-X.
- 471 Smithro, C. G., and S. C. Solomon (2008), An improved parameterization of thermal elec-  
472 tron heating by photoelectrons, with application to an x17 flare, *Journal of Geophysical*  
473 *Research*, *113*, A08,307, doi:10.1029/2008JA013077.
- 474 St-Maurice, J.-P., and W. Hanson (1982), Ion frictional heating at high latitudes and its  
475 possible use for an in situ determination of neutral thermospheric winds and tempera-  
476 tures, *Journal of Geophysical Research: Space Physics (1978–2012)*, *87*(A9), 7580–7602.
- 477 Strangeway, R. J. (2012), The equivalence of joule dissipation and frictional heating in  
478 the collisional ionosphere, *Journal of Geophysical Research: Space Physics (1978–2012)*,  
479 *117*(A2).
- 480 Swartz, W. E., and J. S. Nisbet (1972), Revised calculations of f region ambient electron  
481 heating by photoelectrons, *Journal of Geophysical Research*, *77*, 6259–6261, doi:10.  
482 1029/JA077i031p06259.
- 483 Thayer, J. (1998), Height-resolved Joule heating rates in the high-latitude e region and  
484 the influence of neutral winds, *Journal of Geophysical Research: Space Physics (1978–*  
485 *2012)*, *103*(A1), 471–487.

- 486 Thayer, J. P., and J. Semeter (2004), The convergence of magnetospheric energy flux in the  
487 polar atmosphere, *Journal of Atmospheric and Solar-Terrestrial Physics.*, *66*, 807–824,  
488 doi:10.1016/j.jastp.2004.01.035.
- 489 Torr, M., D. Torr, and P. Richards (1980), The solar ultraviolet heating efficiency of the  
490 midlatitude thermosphere, *Geophysical Research Letters*, *7*(5), 373–376.
- 491 Torr, M. R., D. Torr, P. Richards, and S. Yung (1990), Mid-and low-latitude model of  
492 thermospheric emissions: 1.  $\text{o}^+$  ( $^2\text{p}$ ) 7320 Å and  $\text{n}2$  ( $2\text{p}$ ) 3371 Å, *Journal of Geophysical*  
493 *Research: Space Physics (1978–2012)*, *95*(A12), 21,147–21,168.
- 494 Vichare, G., A. J. Ridley, and E. Yigit (2012), Quiet-time low latitude ionospheric electro-  
495 dynamics in the non-hydrostatic global ionospherethermosphere model, *Journal of At-*  
496 *mospheric and Solar-Terrestrial Physics.*, *80*, 161–172, doi:10.1016/j.jastp.2012.01.009.
- 497 Weimer, D. R. (2005), Improved ionospheric electrodynamic models and application to  
498 calculating Joule heating rates, *Journal of Geophysical Research*, *110*, doi:10.1029/  
499 2004JA010884.
- 500 Zhu, X., E. R. Talaat, J. B. H. Baker, and J.-H. Yee (2005), A self-consistent derivation  
501 of ion drag and Joule heating for atmospheric dynamics in the thermosphere, *Annals of*  
502 *Geophysics*, *23*, 3313–3322, doi:10.5194/angeo-23-3313-2005.

**Figure 1.** The evolution of the global averaged neutral temperature over three simulation days beginning from 00 UT Dec 24, 2012. The solid line shows the simulation using the complete neutral-ion collisional heating rate with PHE equal to zero (termed as the Complete simulation). The dotted line shows the simulation using the Joule heating rate with PHE equal to zero (termed as the Joule simulation). The dashed line shows the simulation using the Joule heating rate with PHE equal to 0.05 (termed with the Joule simulation with 0.05 PHE).

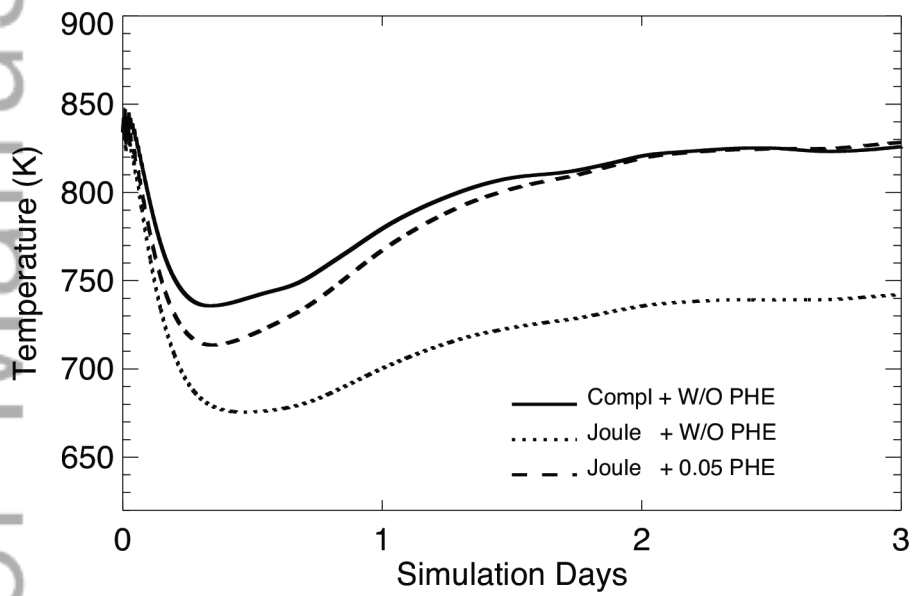
**Figure 2.** The comparison of  $T_n$  between the Complete simulation (left column), the Joule simulation (middle column) and the Joule simulation with 0.05 PHE (right column) at 00 UT on Dec 24, 2012. The top row shows the 300-km altitude slice. The second row shows the 180° longitudinal slice. The bottom row shows the north polar cap above 50° latitude.

**Figure 3.** The percentage difference of  $T_n$  between the Complete and the Joule simulations, i.e.,  $T_n\% = \frac{(T_n)_C - (T_n)_J}{(T_n)_C} \times 100\%$ , at 140 km (top), 250 km (middle) and 400 km (bottom).

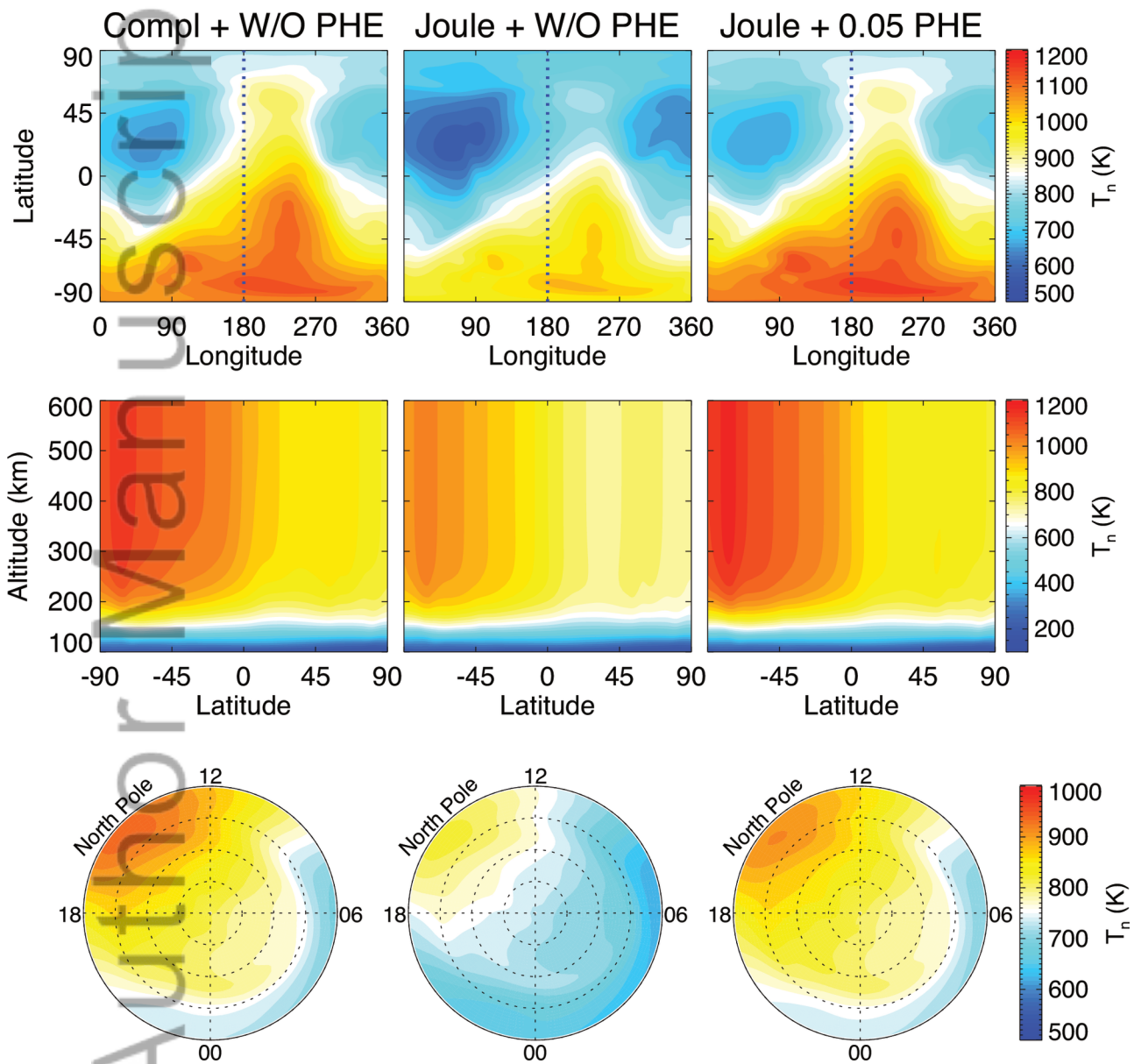
**Figure 4.** The color contour shows the difference of the time rate of change of  $T_n$  due to the neutral-ion energy coupling between the Complete and Joule simulations at 140 km (top), 250 km (middle) and 400 km (bottom). The unit is in  $\text{K} \cdot \text{m}^{-3} \cdot \text{s}^{-1}$ . The dotted line contours the term on the right side of Equation 17.

**Figure 5.** The altitudinal profiles of the ion-electron heat transfer rate (blue), the ion-neutral frictional heating rate (yellow) and the negative ion-neutral heat transfer rate (orange) at three geographic locations at 00 UT of the last day of the simulation.

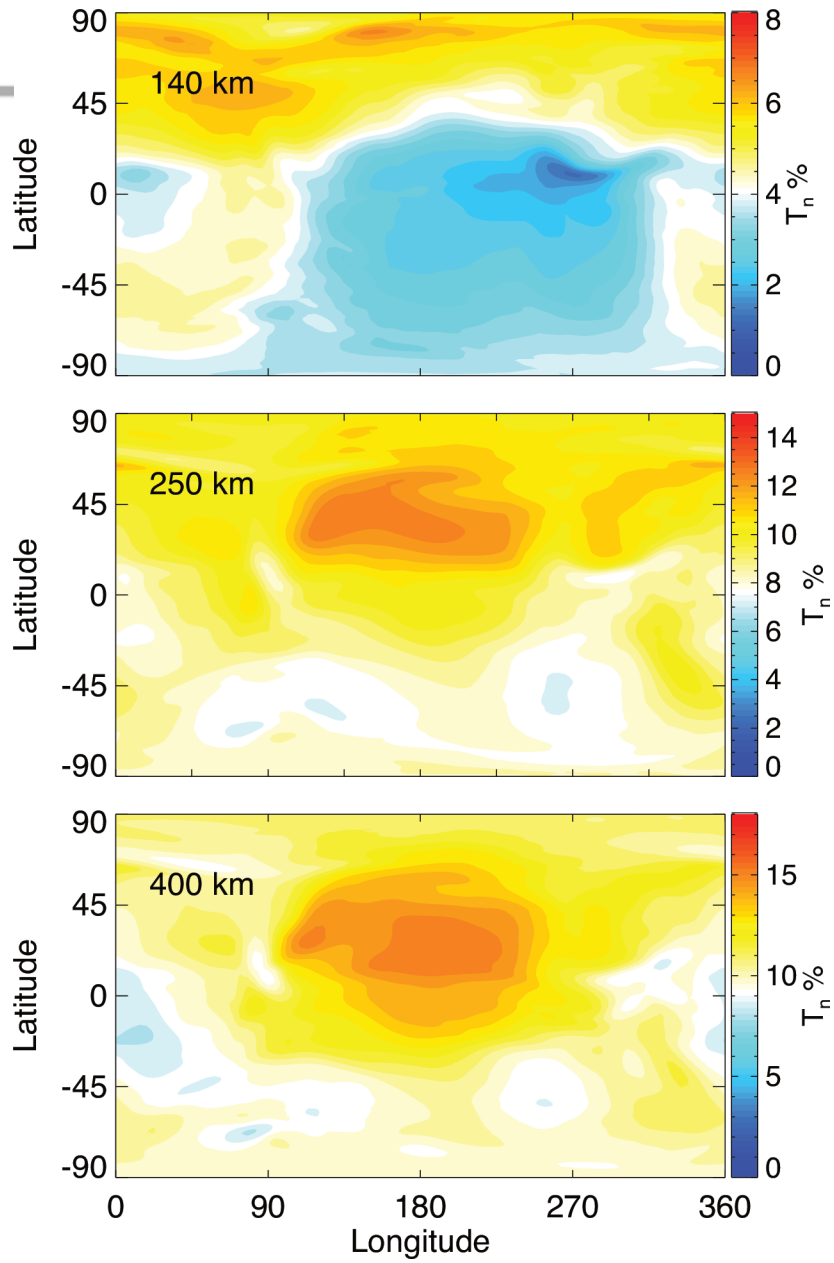
**Figure 6.** In the same format as Figure 1. The left and right panels show the temporal evolution of the global averaged  $T_n$  when  $F10.7 = 70$  sfu and  $F10.7 = 150$  sfu respectively.



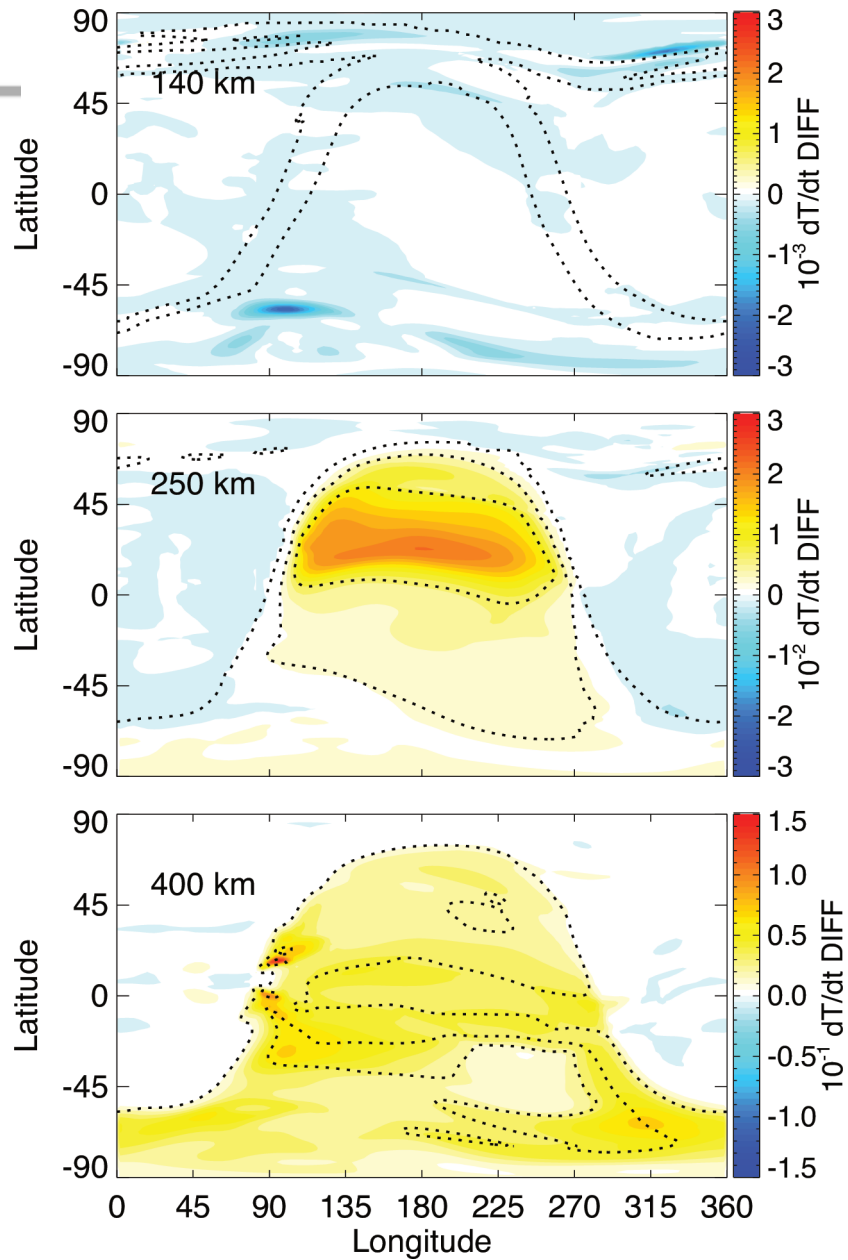
2015ja021637-f01-z-bw



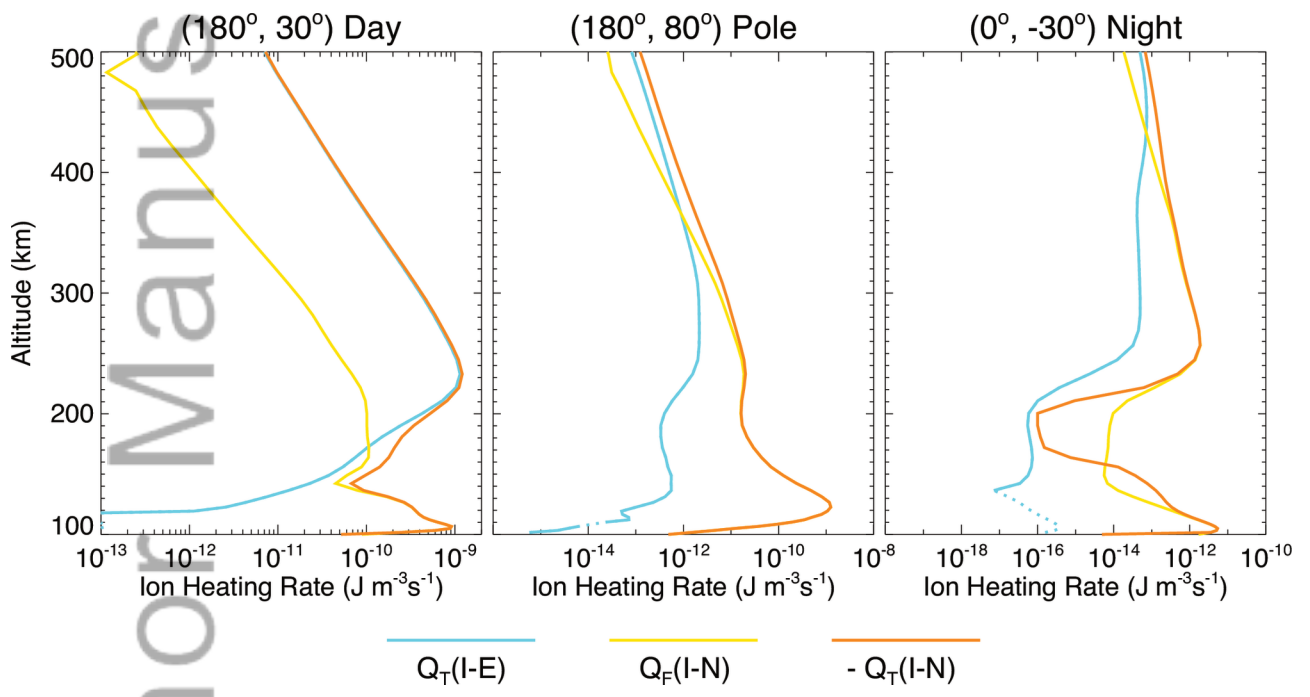
2015ja021637-f02-z-



2015ja021637-f03-z-

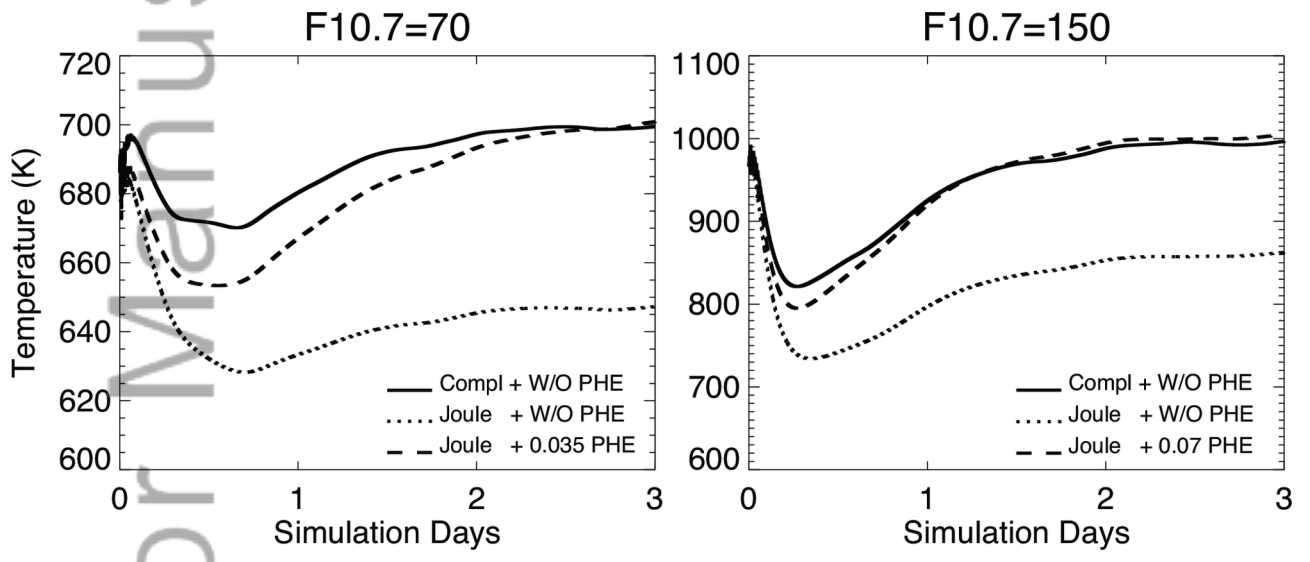


2015ja021637-f04-z-



2015ja021637-f05-z-





2015ja021637-f06-z-bw